Asymmetric transmission-induced probe-configuration-dependent dephasing in an Aharonov-Bohm ring

Kuan-Ting Lin, Yiping Lin, C. C. Chi, and J. C. Chen
Department of Physics, National Tsing Hua University, Hsinchu 30013, Taiwan
(Received 20 September 2011; published 1 December 2011)

We investigate the dephasing rates in quasiballistic Aharonov-Bohm (AB) rings with local- and nonlocal-probe configurations by tuning the transmission through one arm of the ring. The dephasing rates are independent of the probe configuration while the transmissions through the ring paths are equal. In contrast, as AB interferometers are tuned to be strongly asymmetric, the dephasing rate of the local configuration becomes larger than that of the nonlocal configuration. We find that our observations can be qualitatively explained by voltage fluctuations from the measurement circuit, as proposed by G. Seelig, S. Pilgram, A. N. Jordan, and M. Büttiker [Phys. Rev. B **68**, 161310(R) (2003)].

DOI: 10.1103/PhysRevB.84.235404 PACS number(s): 73.23.Ad, 73.63.Nm

Various quantum interference phenomena reveal the wave nature of charges in mesoscopic conductors. One of the best-known demonstrations is the observation of the nonlocal relationship between the electric field and the current density in a ballistic conductor, including Aharonov-Bohm (AB) oscillations in disordered metal rings[1,2] and ballistic rings,[3] the length dependence of voltage fluctuations,[4] the appearance of multiprobe resistance reflecting the Onsager symmetries,[5–7] and weak localization amplitude and Hall resistance in quantum wires.[8,9] As long as the phase coherence of the electron wave can be preserved over the device size, the electron can propagate coherently into the voltage and current probes; consequently, quantum interference appears in the conductance regardless of how the probes are attached to the samples.

Recently, Kobayashi and coworkers found that the decoherence rate (Γ_ϕ) in the local configuration is considerably larger than it is in the nonlocal configuration of a four-terminal AB ring.[3] Despite the nonlocal nature of the resistance revealed in numerous mesoscopic systems, the origin of the dependence of the decoherence properties on the measurement configuration remains unclear. Seelig *et al.* introduced a phase-breaking mechanism to illustrate how a probe-configuration-dependent dephasing rate can occur in a (reflectionless) Mach-Zehnder interferometer (MZI).[10,11] Their theory concluded that the measurement circuits impose different electrical constrains on voltage fluctuations residing in the ring path. As a result, if the transmissions of two ring paths are asymmetric, Γ_ϕ in the local configuration can be larger than that in the nonlocal configuration. The understanding of the influence of the measurement circuit on the transmission phase would be crucial in the manipulation of coherent states in quantum electronics.

It is the aim of this work to investigate the dependence of Γ_ϕ of an AB interferometer in both local and nonlocal probe configurations by tuning the transmission through one of the ring paths. We find that Γ_ϕ continuously evolves with respect to the symmetry of the transmissions. If the transmissions are symmetric, the decoherence rate is independent of the probe configuration. In contrast, larger decoherence is observed in the local measurement when one of the ring paths is gradually closed. We discuss the relevance of our observations to Seelig *et al.*'s theoretical expectations.[11]

The AB ring device is fabricated on a GaAs/AlGaAs heterostructure grown by molecular-beam epitaxy and has a two-dimensional electron gas (2DEG) located 80 nm beneath the surface. The AB ring is prepared by electron-beam lithography and wet etching. A pair of Au/NiCr gates is deposited adjacent to the ring to modify the interference conditions. A scanning electron micrograph of the device is shown in Fig. 1(a). The average ring diameter is $\sim$1.6 μm, and the width of the wire is $\sim$470 nm. The electron density of the ring devices is $n = 2.3\times10^{11}$ cm^{-2} and the mobility is $\mu = 2.1\times10^5$ cm^2/Vs, deduced from Shubnikov–de Haas oscillations at 4.2 K. The electron mean-free path (l_e) is thus estimated to be $\sim$2.2 μm, comparable to the ring size; therefore, the transport through the ring is within the quasiballistic regime.

Measurements were made in a dilution refrigerator with a base temperature of 20 mK. The standard lock-in technique, with an ac excitation current of 10 nA at 17 Hz, was employed in the four-probe setup. We investigated two samples with identical layouts; both samples showed consistent behaviors. Due to space limitations, data obtained from only one sample are presented in detail in this paper. The AB magnetoresistance oscillations were measured in the local and nonlocal configurations, as illustrated in the insets of Figs. 1(c) and 1(d). The terms "local and nonlocal resistance" used here refer to the relative locations of the voltage probes with respect to the current probes, in terms of classical circuitry. A local resistance R_l (nonlocal resistance R_{nl}) is defined as the ratio of the voltage V, measured between contact 3 and contact 2 (4) to the constant current I between contact 1 and contact 4 (2). Note that our recent studies discovered that a large biasing current introduces additional decoherence.[12] A small applied I is essential to correctly compare the dephasing rate in different probe setups. Because R_{nl} can be much less than R_l, extra care has been taken in extracting the dephasing rates from R_{nl}.

To demonstrate gate modulation of the transmission, Fig. 1(b) displays R_l as a function of the gate voltage (V_g) applied to the gate near the lower branch of the ring path. The irregular small fluctuations on R_l are reproducible, and are attributed to the variance of the resonant interference associated with the change of the geometry of the wave guide as V_g is varied. R_l remains qualitatively unchanged for V_g larger than a threshold voltage $V_t \sim -0.06$ V.

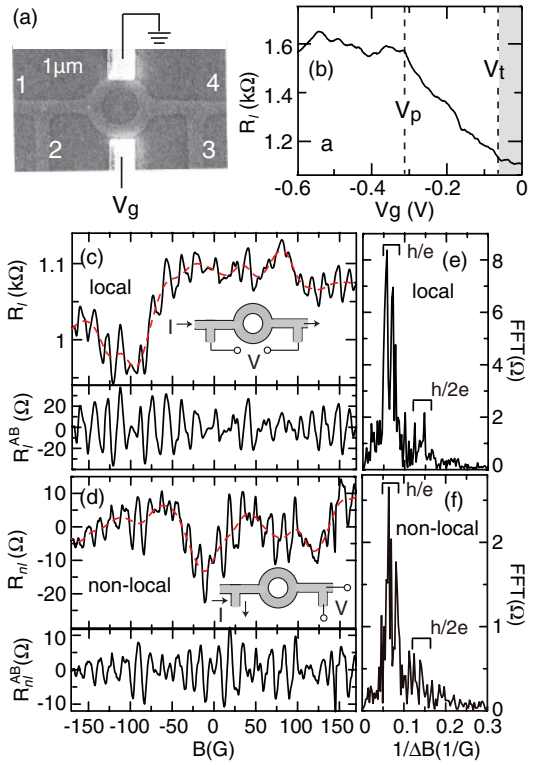

FIG. 1. (Color online) (a) SEM micrograph of the AB ring structure. (b) The four-probe resistance R_l vs V_g. The dashed line marks the threshold voltage of depletion ($V_t \sim -0.06$ V) and the pinch-off voltage ($V_p \sim -0.3$ V), below which the transmission of the lower path is cut. (c), (d) The upper panels represent the magnetoresistance of R_l and R_{nl} measured in the local and nonlocal setup, respectively. The red dashed lines are used to indicate the background resistance. The insets depict the probe configurations of the local and nonlocal setups. The lower panels of (c) and (d) show the local and the nonlocal AB oscillation, R_l^{AB} and R_{nl}^{AB}, after subtracting the background resistance, respectively. (e), (f) The Fourier spectrum of the data corresponding to (c) and (d), respectively.

It then increases monotonically until V_g has fallen to -0.3 V, and levels off at approximately 1.6 kΩ for $V_g < -0.3$ V. This result suggests that the transmission of the lower ring path is turned off at a pinch-off voltage $V_p \sim -0.3$ V.

Figures 1(c) and 1(d) show the magnetoresistances R_l and R_{nl}, respectively, at $V_g = 0$ V. As the magnetic field B is ramped, clear periodic oscillations appear superimposed on a more smoothly varying background (marked by the red dashed lines). The traces of AB oscillations, denoted as R_l^{AB} and R_{nl}^{AB} for the local and nonlocal setup, are obtained by subtracting the background from the raw magnetoresistance curves, as shown in the lower panels of Figs. 1(c) and 1(d). In the Fourier power spectra of R_l^{AB} and R_{nl}^{AB} [Figs. 1(e) and 1(f)], the period of the high-frequency oscillations is approximately $\Delta B \sim 16$ G, consistent with the addition of the flux $\Phi_0 = h/e$ through the hole. The amplitudes of the AB oscillations ΔR_{AB} are estimated by integrating the spectra over the width of the h/e peak.

R_l and R_{nl} exhibit pronounced asymmetric magnetoresistance with respect to $B = 0$ T, as shown in Figs. 1(c) and 1(d).

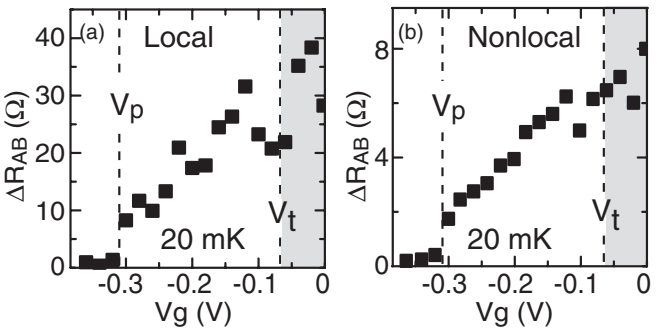

FIG. 2. AB oscillation ΔR_{AB} vs V_g for the (a) local and (b) nonlocal configuration. ΔR_{AB} vanishes when $V_g \sim V_p$. The error bars are comparable to the symbol size.

Moreover, negative resistance is found in R_{nl}. Both phenomena can be understood in terms of quantum interference effects or bending of ballistic electrons,[13–16] and thus they provide further evidence of the ballistic nature of our devices. It is known that ballistic transport is extremely sensitive to the details of the spatial potential in microstructures, varying with the sample geometry and the measurement geometry. In our experiments, the typical value of R_l (∼1 kΩ) is much larger than that of $|R_{nl}|$, ∼10 Ω. The channel number (N) residing in the wire can be estimated to be about $N \sim 12$. Considering a phase-coherent four-terminal conductor with the geometry shown in Fig. 1(a) and neglecting the interchannel coupling, the Landauer-Büttiker (L-B) formula gives

$$R_l \approx \frac{h}{2e^2}\frac{T_{12}-T_{13}}{(T_{23}+T_{13})(T_{12}+T_{23})}, \tag{1a}$$

$$R_{nl} \approx \frac{h}{2e^2}\frac{T_{23}-T_{13}}{(T_{12}+T_{13})(T_{12}+T_{23})}, \tag{1b}$$

for the local and nonlocal configurations, respectively.[17] Here, T_{mn} represents the probabilities for carriers incident on the m lead to be transmitted to the n lead. We approximate the symmetric transmissions at $V_g = 0$ as $T_{12} = T_{21} = T_{43} = T_{34}$, $T_{23} = T_{32} = T_{14} = T_{41}$, $T_{13} = T_{31} = T_{42} = T_{24}$. Based on the ring geometry, we further assume $T_{12} \gg 1$ and $T_{12} > T_{23} \sim T_{13}$. It can be readily seen that Eqs. (1a) and (1b) qualitatively explain the observed $R_l \gg R_{nl}$.

Figure 2 displays the gate-voltage dependence of ΔR_{AB}, measured at 20 mK. We observe that ΔR_{AB} of both probe configurations exhibits irregular variation as $V_g \geqslant V_t$. The variation of ΔR_{AB} with V_g suggests that even before the start of the 2DEG depletion, the applied V_g changes the electrostatic potential in one arm of the ring; hence, interference patterns subtly vary in response to the induced phase shifts.[3,18] When a less negative V_g is applied ($V_g < V_t$), ΔR_{AB} monotonically decreases with V_g. Finally, ΔR_{AB} disappears as $V_g = V_p$ is reached.

Figure 3 shows the temperature (T) dependence of ΔR_{AB} for different V_g in local and nonlocal setups. Disregarding the probe setup, ΔR_{AB} saturates for $T \leqslant 100$ mK. The mechanism of the quantum phase saturation at low temperatures remains an important but poorly understood issue worthy of investigation.[19] This issue is left for future studies. In this work, we only focus on ΔR_{AB} above approximately 200 mK, where ΔR_{AB} decreases with increasing T in both probe

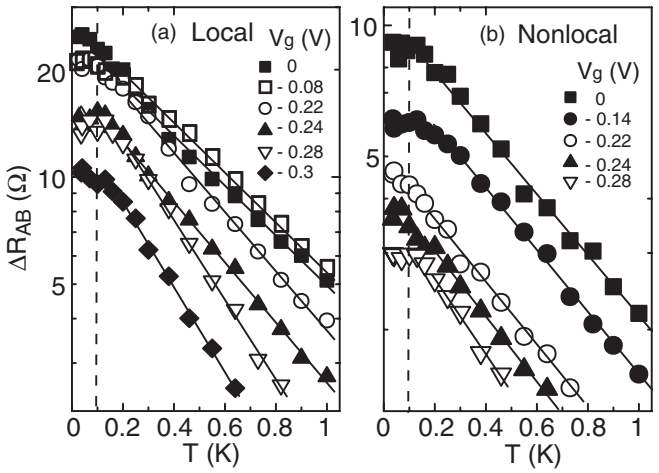

FIG. 3. Temperature dependence of the AB amplitude (ΔR_{AB}) of the h/e at different applied voltages (V_g) in (a) the local configuration and (b) the nonlocal configuration. The solid lines are the results of fits to the data using the exponential relationship discussed in the text. The dashed line marks the onset of the linear fit. ΔR_{AB} saturates for the temperatures below the dashed line.

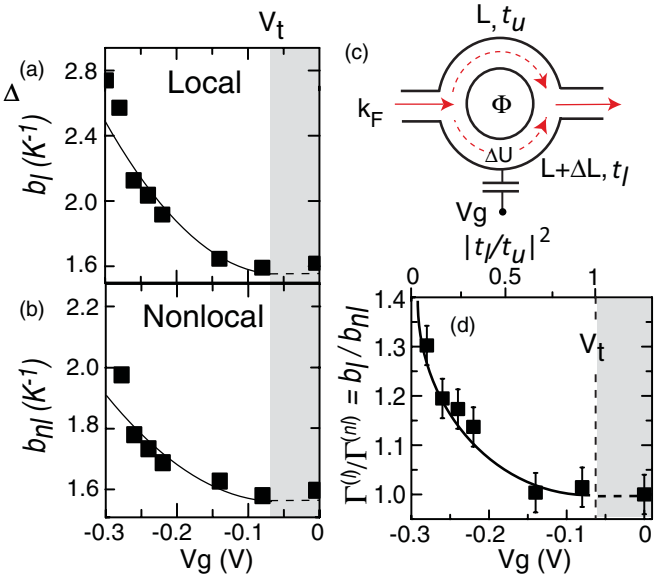

FIG. 4. (Color online) Exponents b_n and b_{nl} extracted from the measured data in Fig. 3 vs V_g for (a) the local and (b) the nonlocal setup. The solid lines represent a fit with $b_n = 15.3(V_g - V_t)^2 + 1.57$ and $b_{nl} = 6.5(V_g - V_t)^2 + 1.57$ for $V_g < V_t$. The sizes of the symbols shown in (a) and (b) reflect the error bars. (c) A schematic diagram illustrating the AB-ring geometry. (d) The ratio of b_n and b_{nl} vs V_g, or the relative transmissions of the upper and lower paths. The data points are connected by an eye-guiding line.

configurations. Phenomenologically, we can fit ΔR_{AB} with an exponential decay function of the temperature: $\Delta R_{AB} \propto \exp(-b_{l(nl)}T)$, where b_l (b_{nl}) is the fitting parameter and reflects the damping rate of the AB amplitude with T in the local (nonlocal) setup. The straight lines shown in Figs. 3(a) and 3(b) are fitted results for T in the range of 200 mK to 1 K. Figures 4(a) and 4(b) summarize b_n and b_{nl} as a function of V_g. As $V_g > V_t$, the decay rate of ΔR_{AB} becomes independent of V_g despite the observed substantial variance of ΔR_{AB} with V_g (as shown in Fig. 2). For $V_g < V_t$, we find that the increases of both b_n and b_{nl} with V_g can be fitted by a function of the form $(V_g - V_t)^2$, as shown in the solid lines in Figs. 4(a) and 4(b).

We now wish to explain our findings. The ring geometry of our system is shown in Fig. 4(c). Here, L and $L + \Delta L$ represent the length of the upper and lower arms, respectively. Biasing the side gate on the lower arm introduces not only an extra path difference (ΔL) due to the finite width of the ring, but also a change of the internal potential ΔU. Electrons injecting through the ring carry a wave vector k around the Fermi wave vector k_F for small biasing currents. The transmission probability $T_{m,n}$ for those (n,m) that cross the ring, then, can be written as

$$T_{m,n} = T_1 + 2t_l t_u \cos\left(k_F \Delta L + \Delta U \tau_L/\hbar + 2\pi \frac{\Phi}{\Phi_0}\right); \quad (2)$$

T_1 accounts for the flux-insensitive transmission probability, and t_l and t_u are the transmission amplitudes of the lower and upper arms, respectively. $\tau_L = L/v_F$ is the transit time of electrons through a ring arm, and v_F is the Fermi velocity. Φ is the magnetic flux threading the ring. We treat t_u as a constant and t_l as a linear function of V_g. Because $t_l \sim t_u$ at $V_g > V_t$ and $t_l = 0$ at $V_g = V_p$, we can reasonably assume that the transmission probability depends linearly on the gate voltage in the voltage range between V_p and V_t; i.e., $|t_l/t_u|^2 = (V_g - V_p)/(V_t - V_p)$.

The coherent quantum states are inevitably perturbed by the various external fluctuations in the system. Decoherence occurs for those fluctuations taking place on a time scale shorter than τ_L. The reduction of ΔR_{AB} in a ballistic ring has been attributed to either the thermal averaging effect[20] or quantum decoherence induced by electron-electron (e-e) interactions.[10,21] Considering the phase term $k_F \Delta L$ in Eq. (2) at finite temperature, thermal fluctuation induced dephasing can be evaluated by the ratio of the thermal broadening energy $k_B T$ and a characteristic energy $E_c = 2E_F/(k_F \Delta L)$, where E_F is the Fermi energy, and k_B is the Boltzmann constant. In principle, the thermal averaging effect is independent of the probe configuration. On the other hand, to account for the effects of ΔU in dephasing, the fluctuating nature of ΔU must be specified. Seelig and Büttiker suggest that the decoherence induced by the fluctuations of ΔU can result from the charge fluctuations between the ring and the nearby side gates through e-e interactions.[10]

R_l and R_{nl} can be obtained by taking the average of the fluctuations by summing T_{mn} over all contributing channels through the L-B formula. From Eqs. (1a) and (1b), the AB amplitude can be extracted as

$$\Delta R_{AB} \propto t_l t_u^* e^{-\tau_L \Gamma_\phi}, \quad (3)$$

where Γ_ϕ can be defined as $\Gamma_\phi = \gamma_{th} + \gamma_e$. Here, $\gamma_{th} = k_B T/\hbar$ is the dephasing rate from the thermal averaging effect, and γ_e is the dephasing rate due to e-e interactions, in which $\gamma_e \propto T$ is theoretically proposed.[10] Because both γ_{th} and γ_e exhibit linear T dependence, it is difficult to distinguish the contributions of γ_{th} and γ_e in Γ_ϕ from the results of T-dependent experiments.

Comparing Γ_ϕ with the experimental results, we can obtain $\Gamma_\phi^l \propto b_l T$ and $\Gamma_\phi^{nl} \propto b_{nl} T$ as a function of V_g, where $\Gamma_\phi^{l(nl)}$

denotes the dephasing rate for local (nonlocal) setup. The trends $\Gamma_\phi^{n(nl)} \propto T$ for $T > 100$ mK shown in Fig. 3 are in agreement with the results of previous studies.[3,12,22] The good exponential fit of ΔR_{AB} with T implies that $t_l t_u^*$ is insensitive to T for 1.2 K $> T >$ 100 mK.

We then focus on $\Gamma_\phi^{l(nl)}$ as a function of the transmission amplitude t_l. From the fitting results of Figs. 4(a) and 4(b), we can obtain $\Gamma_\phi^l \propto b_l = 0.88(|t_l/t_u|^2 - 1)^2 + 1.57$ and $\Gamma_\phi^{nl} \propto b_{nl} = 0.37(|t_l/t_u|^2 - 1)^2 + 1.57$. Figure 4(d) shows the ratio of the decoherence rates, $\Gamma_\phi^l/\Gamma_\phi^{nl} = b_l/b_{nl}$. As $V_g \leqslant V_t$, $t_l \sim t_u$ and $\Gamma_\phi^l/\Gamma_\phi^{nl} \sim 1$. The dephasing rate is insensitive to the probe configuration, consistent with our previous report in a symmetric AB ring.[12] Intriguingly, when t_l is tuned to be smaller than t_u for less negative V_g, Γ_ϕ^l becomes larger than Γ_ϕ^{nl}. Within the accuracy of our measurements $\Gamma_\phi^l/\Gamma_\phi^{nl}$ is found to increase up to 1.33 (until $V_g \sim V_p$). Buchholz *et al.* investigated the dephasing rates in multichannel asymmetric AB rings, designed with $\Delta L \sim$1.3 μm.[23] They found that the corresponding $b_l \sim 1.44$, $b_{nl} \sim 1.16$, and $\Gamma_l/\Gamma_{nl} \sim 1.24$, quantitatively comparable to our observations.

To interpret the probe-dependent Γ_ϕ, Seelig *et al.* proposed that the decoherence can be attributed to two sources: ΔU fluctuations and voltage fluctuations ΔV_α associated with each lead α. The fluctuations of ΔU and ΔV_α must balance the charge fluctuations inside the ring. Because the charge fluctuations at each lead are directly connected to the arrangement of the voltage probes and the current leads,[11] γ_e can be probe dependent; i.e., $\gamma_e = \gamma_e^0 + \gamma_e^{l(nl)}$. Here, γ_e^0 is the dephasing term irrelevant to probe setup.[10] The magnitude of $\gamma_e^{l(nl)}$ turns out to depend strongly on the symmetry of the interferometer $|t_l/t_u|^2$, AB-unrelated parallel transmission T_0, and backscattering from the interactions ϵ. For a perfectly symmetric ring, $t_l = t_u$, $\gamma_e = \gamma_e^0$. Nevertheless, $\gamma_e^l > \gamma_e^{nl}$ when the transmission becomes asymmetric. The difference between γ_e^l and γ_e^{nl} decreases with the increase of T_0 and ϵ.

The upper scale of Fig. 4(d) replots $\Gamma_\phi^l/\Gamma_\phi^{nl}$ as a function of $|t_l/t_u|^2$. The increase of $\Gamma_\phi^l/\Gamma_\phi^{nl}$ associated with the decrease of $|t_l/t_u|^2$ qualitatively substantiates the predictions of Seelig *et al.* The value $b_{nl} \sim b_l \sim 1.57$ K^{-1} as $|t_l/t_u| \sim 1$ regardless of the probe setup could be attributed to $\gamma_{th} + \gamma_e^0$. We can estimate the decoherence related to γ_{th} by $b = \tau_L k_B/\hbar \sim 1$ K^{-1}. Because the value of b obtained by thermal averaging effects is comparable to the measured value of $b_{l(nl)}$, most previous studies suggest that the decoherence could be dominated by γ_{th}.[3,12,23] However, the probe-dependent term related to the transmission ratio $|t_l/t_u|^2$ in $\Gamma_\phi^{l(nl)}$ could be attributed to γ_e, but not to γ_{th}. Considering the dephasing mechanism proposed by Seelig *et al.*, we can evaluate the scale of the decoherence induced by *e*-*e* interaction as $b_\phi^l - b_\phi^{nl} \sim 0.59 \pm 0.06$ K^{-1} at T = 100 mK.

Seelig *et al.* consider the dephasing through the internal potential fluctuations alone. In our experiments, as V_g approaches V_p, k of the lower arm is much less than k_F in the upper arm. Instead of ΔU alone, fluctuations of $\Delta(kL)$ involving both ΔU and ΔL must be taken into account in calculating Γ_ϕ. It is important to note that the role of channel coupling in dephasing remains to be clarified. Moreover, uniform potential fluctuations inside the ring will not give rise to different dephasing rates for different probe setups. A path-specific dephasing mechanism that manifests in asymmetric transmissions is necessary to derive probe-dependent dephasing rates.

It is worth noting that geometrical dependence of decoherence has been both theoretically and experimentally found on diffusive systems, where *e*-*e* interaction is considered to be the dominant phase-breaking mechanism.[24–27] For a diffusive (or a metallic) ring, theory developed in Ref. 24 suggests that the dephasing rate is determined by an energy transfer process, dependent on the ring radius.[24] Although distinct features attributed to a ballistic quantum wire were observed in our experiments as shown in Figs. 1(c) and 1(d), we cannot completely rule out the contributions of the diffusive components in both R_l and R_{nl}. However, a detailed analysis to see how these effects might relate to our observations needs further theoretical investigations and is beyond the scope of the present work.

In summary, we investigated the dephasing rates in an AB ring by tuning the transmission of a ring path in different probe configurations. We find that for a symmetric ring, the dephasing rate shows no difference for different measurement configurations; however, the dephasing rate in the local setup begins to exceed that of the nonlocal setup as the transmission becomes more asymmetric. Our results provide compelling evidence for the direct observations of decoherence induced by *e*-*e* interactions in a controlled manner.

We acknowledge Markus Büttiker, the late Mikhail Polianski, and Chung-Yu Mou for valuable discussions. J. C. Chen thanks the National Center for Theoretical Sciences in Taiwan for considerable help. This work is supported by the National Science Council (Grant No. NSC 95-2112-M-007-049-MY3) in Taiwan.

[1] C. P. Umbach, P. Santhanam, C. van Haesendonck, and R. A. Webb, Appl. Phys. Lett. **50**, 1289 (1987).
[2] R. A. Webb and S. Washburn, Phys. Today **41**(12), 46 (1988).
[3] K. Kobayashi, H. Aikawa, S. Katsumoto, and Y. Iye, J. Phys. Soc. Jpn. **71**, 2094 (2002).
[4] M. Büttiker, Phys. Rev. B **35**, 4123 (1987).
[5] H. U. Baranger, A. D. Stone, and D. P. DiVincenzo, Phys. Rev. B **37**, 6521 (1988).
[6] C. L. Kane, P. A. Lee, and D. P. DiVincenzo, Phys. Rev. B **38**, 2995 (1988).
[7] S. Hershfield and V. Ambegaokar, Phys. Rev. B **38**, 7909 (1988).
[8] V. Chandrasekhar, D. E. Prober, and P. Santhanam, Phys. Rev. Lett. **61**, 2253 (1988).
[9] A. D. Stone and A. Szafer, IBM J. Res. Dev. **32**, 384 (1988).
[10] G. Seelig and M. Büttiker, Phys. Rev. B **64**, 245313 (2001).
[11] G. Seelig, S. Pilgram, A. N. Jordan, and M. Büttiker, Phys. Rev. B **68**, 161310 (2003).
[12] K.-T. Lin, Y. Lin, C. C. Chi, J. C. Chen, T. Ueda, and S. Komiyama, Phys. Rev. B **81**, 035312 (2010).
[13] S. Washburn and R. A. Webb, Adv. Phys. **35**, 375 (1986).

[14]G. Timp, A. M. Chang, P. Mankiewich, R. Behringer, J. E. Cunningham, T. Y. Chang, and R. E. Howard, Phys. Rev. Lett. **59**, 732 (1987).
[15]H. U. Baranger and A. D. Stone, Phys. Rev. B **40**, 8169 (1989).
[16]Y. Takagaki, K. Gamo, S. Namba, S. Ishida, S. Takaoka, K. Murase, K. Ishibashi, and Y. Aoyagi, Solid State Commun. **68**, 1051 (1988).
[17]M. Büttiker, Phys. Rev. Lett. **57**, 1761 (1986).
[18]P. G. N. de Vegvar, G. Timp, P. M. Mankiewich, R. Behringer, and J. Cunningham, Phys. Rev. B **40**, 3491 (1989).
[19]J. J. Lin and J. P. Bird, J. Phys. Condens. Matter **14**, R501 (2002).
[20]M. Cassé, Z. D. Kvon, G. M. Gusev, E. B. Olshanetskii, L. V. Litvin, A. V. Plotnikov, D. K. Maude, and J. C. Portal, Phys. Rev. B **62**, 2624 (2000).
[21]M. Büttiker, IBM J. Res. Dev. **32**, 317 (1988).
[22]A. E. Hansen, A. Kristensen, S. Pedersen, C. B. Sorensen, and P. E. Lindelof, Phys. Rev. B **64**, 045327 (2001).
[23]S. S. Buchholz, S. F. Fischer, U. Kunze, M. Bell, D. Reuter, and A. D. Wieck, Phys. Rev. B **82**, 045432 (2010).
[24]T. Ludwig and A. D. Mirlin, Phys. Rev. B **69**, 193306 (2004).
[25]M. Ferrier, A. C. H. Rowe, S. Guéron, H. Bouchiat, C. Texier, and G. Montambaux, Phys. Rev. Lett. **100**, 146802 (2008).
[26]C. Texier, P. Delplace, and G. Montambaux, Phys. Rev. B **80**, 205413 (2009).
[27]M. Treiber, C. Texier, O. M. Yevtushenko, J. von Delft, and I. V. Lerner, Phys. Rev. B **84**, 054204 (2011).